Visualization of X-ray Beam Using $CdWO_4$ Crystal for Macromolecular Crystallography

Kazimierz J. GOFRON and Andrzej JOACHIMIAK
Structure Biology Center,
Biosciences Division, Argonne National Laboratory,
Argonne, Illinois 60439, USA

ABSTRACT

In synchrotron diffraction experiments, it is typically assumed that the X-ray beam at the sample position is uniform, stable and has dimensions that are controlled by the focus and slits settings. As might be expected, this process is much more complex. We present here an investigation of the properties of a synchrotron X-ray beam at the sample position. The X-ray beam is visualized with a single crystal scintillator that converts X-ray photons into visible light photons, which can be imaged using Structure Biology Center (SBC) on-axis and off-axis microscope optics. The X-ray penetration is dependent on the composition of the scintillator (especially the effective Z), and X-ray energy. Several scintillators have been used to visualize X-ray beams. Here we compare $CdWO_4$, $PbWO_4$, $Bi_4Ge_3O_{12}$, $Y_3Al_5O_{12}$:Ce (YAG:Ce), and Gd_2O_2S:Tb (phosphor). We determined that scintillator crystals made of $CdWO_4$ and similar high-Z materials are best suited for the energy range (7–20 keV) and are most suitable for beam visualization for macromolecular crystallography applications. These scintillators show excellent absorption, optical, and mechanical properties.

Keywords: Synchrotron; X-ray; Scintillator; Fluorescence; Single crystal; Gd_2O_2S:Tb; $CdWO_4$; imager; $PbWO_4$; $Bi_4Ge_3O_{12}$; $Y_3Al_5O_{12}$:Ce (YAG:Ce), phosphor.

1. INTRODUCTION

In macromolecular crystallography (MX), the main motivation for crystal visualization at synchrotron beamlines is the accurate positioning of a small crystal sample in the center of the rotation of a goniostat, and the precise alignment of the goniostat center of rotation with the center of the X-ray beam. The visualization approaches have been relying primarily on optical microscopes operating in the visible and UV spectrum range [1]. The challenge originates from the fact that a small 5–50 μm size biological crystal must be placed in the center of the goniostat rotation while the center of a similarly sized X-ray beam impinges upon the goniostat rotation center and the crystal sample. Furthermore, the alignment of the sample with the beam must be maintained while the goniostat is rotated during diffraction data collection. Data collection using mini-beams and data collection for crystals smaller than 10 μm have become highly demanding methods [2]. For optimal X-ray diffraction data collection, a uniform intensity X-ray beam should match the size of the crystal to minimize background and maximize signal-to-noise ratio.

Our X-ray monochromator optics consists of a 1st Si [111] crystal which is a polished hockey-puck design with vertical focusing done by mirror and horizontal focusing done with a polished 30 mm wide unribbed sagitally bent 2nd Si [111] crystal [3]. The beam is typically focused downstream of the sample and upstream of the X-ray CCD detector, resulting in a 200 x 75 μm^2 (FWHM) unslitted X-ray beam. The typical 19-ID X-ray beam used in protein crystallography is adjusted approximately to the size of the crystal under study, using slits.

The knowledge of the beam size at the sample position is one of the most important experiment parameters. Current tools are insufficient, particularly to image X-ray mini-beams (5–25 μm). Beam sizes of this magnitude are becoming more common at synchrotron facilities. This study focuses on the methods for establishing X-ray beam quality (size, shape and intensity distribution) at the sample position. The current state of the art technique is to use a phosphor layer that responds to X-rays by re-emitting the energy as visible light that is imaged by a microscope. This determines the synchrotron beam position and general beam shape at the sample location. Unfortunately, an X-ray phosphor (such as Gd_2O_2S:Tb) exhibits significant "blooming", and even though it is a great and sensitive tool to determine beam presence and shape, it is not optimal for small X-ray mini-beams. Phosphor is also unsatisfactory for studies of X-ray beam intensity distribution and beam structure due to the non-uniformity of phosphor particles. Moreover, available phosphor pads have varying density, thickness and rough surface, which can lead to inaccurate information about the X-ray beam shape, intensity, and location. The non-coaxial viewing of the X-ray beam requires considerable skills due to the difficulty in the identification of the phosphor depth from which the visible fluorescence radiation emanates. The 3D nature of X-ray fluorescence makes it difficult to ascertain the center of intensity and the X-ray beam shape. With X-ray radiation, the avoidance of parallax error is not as intuitive as it is with visible light radiation, due to the fact that X-rays excite fluorescence throughout the whole volume of the scintillating material. The pursuit of an improved spatial location of the X-ray beam, as well as its size and intensity, is significantly more intuitive with on-axis viewing [2,4,5,6]. For instance, the parallax error is eliminated when viewing coaxially along the beam (on-axis), as shown in Fig. 1.

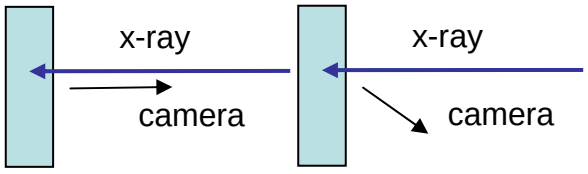

Figure 1: On-axis view (left), and off-axis view (right) in the experiment setup. The off-axis camera has a 38º angle with the x-ray beam direction.

Here we propose the use of single crystal scintillators as a replacement for a phosphor beam monitor/diagnostic tool for macromolecular crystallography facilities at synchrotron sources. The use of a crystal scintillator to visualize a mini-beam was first reported by Perrakis and colleagues who used a bismuth germanate oxide ($Bi_4Ge_3O_{12}$) (BGO) crystal to image a micron-size beam [4]. Here we propose a different crystal material with better properties to image X-ray beams with sizes from a few to hundreds of microns.

The scintillator crystals have to satisfy a number of requirements [7]. They cannot be hygroscopic, due to moisture condensation related to the use of gaseous N_2 and He cryo-stats. This eliminates classes of high efficiency scintillators such as CsI:Tl, CsI:Na, NaCl:Tl. In addition, the crystals should emit in the visible spectrum range – which eliminates very efficient scintillators such as YAP:Ce (yttrium aluminum perovskite activated by cerium) (375 nm emission in near UV). In addition, the ideal scintillator crystals should have a high stopping power (e.g. high atomic number Z) for X-ray energies used in MX (5–20 keV). This is because the image of the beam originating from a deeply penetrating X-ray beam changes the observation perspective of the cross-sectional X-ray beam intensity profile. The high effective Z requirement eliminates excellent scintillators such as YAG:Ce (yttrium aluminum garnet activated by cerium). Scintillators should also be radiation resistant, and scintillate at temperatures used in MX (from 10 to 300 K). Moreover, the scintillation materials should be transparent to their own visible light emission (no self absorption). A list of X-ray scintillators and published references can be found at http://scintillator.lbl.gov/ [7].

Ideally we would like to image visible light fluorescence from a very thin crystal layer (thin compared to a cross-section of the X-ray beam). Such a "thin" scintillation volume eliminates complications related to the 3D nature of the scintillation produced by penetrating X-ray radiation. There are two approaches to achieve synchrotron X-ray mini-beam visualization. One is to have a very thin layer (1–5 μm) of a scintillator crystal (such as YAG:Ce) mounted on a rigid transparent glass slide to visualize scintillation intensity. Very thin scintillator crystals are generally costly, and require mounting on backing materials. In work done by Paris and colleagues, the X-ray beam was visualized on-axis in transmission mode where fluorescent light passes through the scintillator crystal and backing glass in a position where the visualization camera is blocking the X-ray detector [8]. Such beam visualization has a limitation in that it can not be done during data collection. In Yi and colleagues' work, they used a single crystal scintillator to visualize the image of the X-ray diffraction for topography studies [9]. They also used X-ray bright field imaging using crystal scintillators for analyzing crystalline defects [10].

We have tested a different application of the crystal scintillator $CdWO_4$ (CWO), where the X-ray beam is stopped by a thin layer of a scintillator with a high effective Z value. We also visualize the irradiated front of a scintillator crystal in the on-axis position (camera viewing from the X-ray source direction), and unlike in earlier experiments, [8] visible fluorescent light traverses neither the scintillator nor any backing material. Our solution requires neither backing glass nor specially prepared thin scintillator material. There are several scintillator crystals that are well suited for synchrotron X-ray beam visualization. In addition to CWO we are pursuing the use of $PbWO_4$ (PWO) and $Bi_4Ge_3O_{12}$ (BGO) scintillators for X-ray mini-beam visualization and studies of synchrotron beam properties.

2. OPTICAL PROPERTIES OF SCINTILLATOR CRYSTALS

In addition to the scintillator requirements described earlier, the optical properties of scintillator crystals are also very important to X-ray beam visualization. Since visible light is guided through the scintillator, the scintillator material should be transparent to its own radiation. Moreover, CWO, PWO, and BGO scintillators have a very high index of refraction (around 2.1–2.3) in the visible range, and are comparable only to diamond. Fortunately, the high index of refraction causes stray emanating visible fluorescent light to be trapped within the crystal, which helps to obtain better spatial resolution and quenches "blooming". A high index of refraction also makes the image of the X-ray source appear closer to the surface, which improves perceived resolution, as well as limits the cone of accepted emanating fluorescence radiation due to total internal reflection. A high index of refraction also guides stray light to crystal edges, improving contrast ratio.

From the X-ray absorption perspective, these scintillator crystals have a series of absorption edges (W, Bi, and Pb L edges) in the energy range of 11–17 keV, which fully stop X-rays within few microns of the crystal surface (Fig. 2). This makes the depth of emitted visible light quite shallow, as seen in Fig. 5.

The physics of the luminescence in scintillator crystals has been studied due to their extensive application in high energy physics experiments. The studies of PWO by Laguta and colleagues show that blue emission is excitonic in nature and related to the radiative decay of $(WO_4)^{2-}$ [11]. The green emission in PWO has two primary components, of which one is observed at low temperature, while the other is related to Pb and O vacancies.

For many reasons, the scintillation mechanism is not damaged by radiation in PWO crystals [12]; however, optical transmission of the PWO crystal is damaged by radiation. Moreover, an afterglow in PWO is dependent on the irradiation dose rate, and thus only the optical transmission of the crystal is damaged by irradiation. The PWO transmission damage is dose-rate dependent up to some saturation level at which the rate of defect filling by radiation created carriers becomes equal to their release rate. For undoped PWO, crystal radiation induced optical absorption decreases over a period of hours, and optical transmission improves. Doping with a combination of Mo, La, Tb and Y increases the total scintillation yield in the crystal at room temperature.

W	Abs [eV]	Emit [eV]
W K 1s	69,525	59,318
W L1 2s	12,100	11,285
W L2 2p1/2	11,544	9,672
W L3 2p3/2	10,207	8,397

Table 1: Some of the X-ray absorption and emission lines for tungsten.

Cadmium tungstate ($CdWO_4$) is a high density scintillator with a high atomic number and a relatively high light yield. The emission maximum for CWO is at the blue wavelength of 475 nm and the total light output is 12–15 photons/keV. $CdWO_4$ has two emission maxima, one at 470 nm and one at 540 nm. For X-ray irradiation, both components are excited. The decay time of the 470 nm component is 20 μs; the 540 nm component has a 5 μs decay time. The scintillation times are significantly faster than fluorescence times observed for phosphors. The afterglow of $CdWO_4$ upon X-ray irradiation is very low, typically less than 0.1% after 3 ms. The material shows a very good radiation resistance and for doses of 104 Gy (10400 rad) X-rays, the optical transmission of the crystal decreases by less than 15%. Even though some self-absorption of the scintillation light occurs for $CdWO_4$, our use of it for light emanating from the surface will not affect its performance in our application, and the visible light intensity produced is fairly proportional to the X-ray intensity.

Cd	Abs [eV]	Emit [eV]
Cd K 1s	26,711	23,173
Cd L1 2s	4,018	3,717
Cd L2 2p1/2	3,727	3,316
Cd L3 2p3/2	3,538	3,134

Table 2: Some of the X-ray absorption and emission lines for cadmium.

The intensity of the scintillation emission of CWO varies only slightly near room temperature (300 K). Cooling down PWO to between 293 and 253 K enhances the scintillation by a factor of 3 [13]; the luminescence of CWO and BGO increases monotonically when temperature decreases down to 88 K [14]. This enhanced luminescence at lower temperature is a general trend for single crystal scintillators used here (PWO, CWO, BGO), and makes single crystal scintillators work well near 100 K, a typical crystal sample operational temperature of the macromolecular crystallography beamline.

3. X-RAY TRANSMISSION CALCULATIONS

For calculation of the X-ray transmission of the scintillator materials we used the XOP software [15]. The transmission calculations, shown in Fig. 2, demonstrate the stopping power of the particular scintillators. The calculations show that CWO, PWO, BGO, and Gd_2O_2S have high stopping power at 7–17 keV X-ray photon energies. The calculations are not as favorable for the YAG:Ce scintillator, which has a significantly longer X-ray penetration depth. The $CdWO_4$ scintillator material stops X-rays far more effectively in the range of 7–20 keV, than YAG:Ce. The hard X-rays near 12 keV penetrate at least an order of magnitude deeper into the YAG:Ce crystal than into CWO, and this results in the 3D appearance of the X-ray beam image (Fig. 5) obtained from YAG:Ce.

The X-ray transmission calculations in Fig. 2 were done for a Gd_2O_2S powder density of 4.25 g/cm^3, $CdWO_4$ (density 7.9 g/cm^3), BGO (7.13 g/cm^3), $PbWO_4$ (8.2 g/cm^3), and YAG:Ce (4.55 g/cm^3). Despite the fact that solid Gd_2O_2S has a density of about 7.3 g/cm^3, the effective density for X-ray absorption is reduced for the powder form of the material.

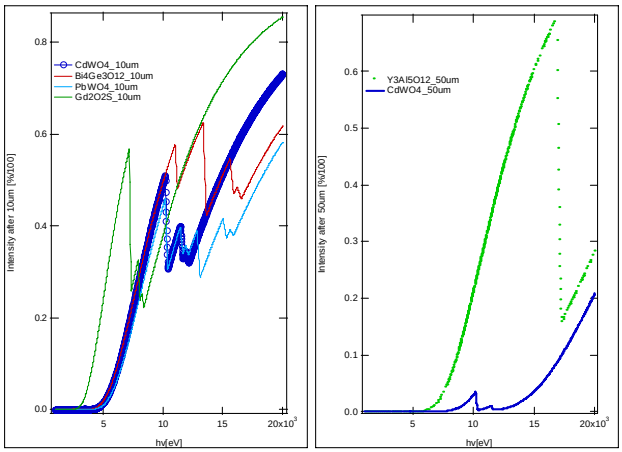

Figure 2: Calculations of the X-ray transmission through 10 μm (left) and 50 μm (right) thicknesses of a material. (left) Transmission through of $CdWO_4$ (blue circle), $PbWO_4$ (light blue), $Bi_4Ge_3O_{12}$ (red), GdO_2S (green). (right) Comparison of $CdWO_4$ (blue) and YAG:Ce (green).

All four high Z scintillator materials (CWO, PWO, BGO, Gd_2O_2S:Tb) appear to have compatible X-ray absorption characteristics with small variations. This is in stark contrast to lower Z material such as YAG:Ce. Even though Gd_2O_2S:Tb has good stopping power for X-rays, and very good light output, the use of this scintillator in powder form limits its usefulness for small X-ray beams imaging due to "blooming" (Fig. 4). The blooming occurs due to propagation of generated visible fluorescence light in the Gd_2O_2S:Tb powder and obfuscates the true beam size and detailed features. Clearly, the use of single crystal scintillators provides significant benefits to X-ray beam visualization. It is worth noting that Gd_2O_2S:Tb is less efficient then CWO in stopping X-rays at energies below Gd L absorption edges (~7.2 keV).

Tables 1 and 2 show the contributions that some of the chemical elements make to X-ray absorption. The extinction length (Table 3) of elements is an indicator of how efficient an element is in absorption, and it is evident that W is one of the most efficient absorbers near 12 keV, as W attenuates intensity to 1/e value over a distance of 2.4 μm.

Element	1/mu @ 12keV [μm]
W	2.37
Cd	14.9
Pb	10.55
Gd	7.36
Bi	11.55
Ge	11.7

Table 3: The extinction lengths of elements used in scintillators [16].

4. X-RAY BEAM: SINGLE CRYSTAL IMAGER

A high quality 10 x 10 x 10 mm^3 single crystal of $CdWO_4$ obtained from Saint-Gobain Crystals [17] was cut into 1 mm [010] oriented wafers, polished on one side, and subsequently diced into 2 x 3 x 1 mm^3 crystals. A small crystal was mounted on a special pin (Fig. 3) using beeswax, with the polished [010]

surface facing toward the X-ray beam. The pin base is made of magnetic steel, and can be mounted magnetically in the same ways as any biological crystal sample is mounted on the MX beamline. The tip of the pin has a semi-circular portion cut out for scintillator crystal mounting. The semi-circular cut-out protects the scintillator crystal from accidental damage, and places it closer to the rotation axis of the pin.

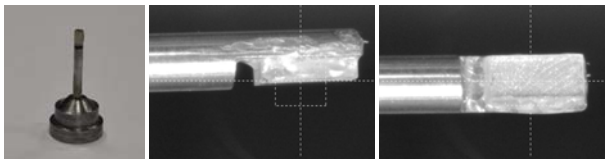

Figure 3: Mounting of a 2 mm x 3 mm $CdWO_4$ single crystal on the "magnetic" base pin. The crystal is attached to the pin with beeswax.

The images (Fig. 4 – right) of the X-ray beam obtained using our $CdWO_4$ single crystal scintillators show the blue component peaking at 475 nm, and spanning monotonically around the peak throughout the visible range from 370 to 750 nm [17].
All scintillator crystals and phosphor were mounted on a pin similar to one shown in Fig. 3, and subsequently mounted on a motorized goniostat.

5. X-RAY MINI BEAM IMAGING

The color images were collected using a Hitachi HV-C20 3CCD camera, YAG:Ce (green) crystal, CWO (blue) crystal, and Gd_2O_2S:Tb (yellow) powder. The Infinity CF3 optics allows an off-axis view that is at 38º with respect to the X-ray beam. The on-axis images are collected using Questar QM-100 microscope [6]. The images displayed in this section were collected at room temperature. In these studies we investigate the X-ray penetration depth and blooming properties. For these studies, our typical X-ray beam was passed further through a 5 µm pinhole located about 50 mm upstream of the X-ray imager. The blooming from Gd_2O_2S:Tb is significantly larger than it is in the case of CWO, as is shown in Fig. 4.

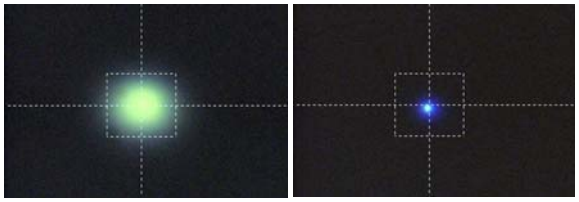

Figure 4: The off-axis (38º with respect to the X-ray beam) view of the synchrotron X-ray (12 keV) beam that passed through a 5 µm pinhole using phosphor (left), and single crystal CWO (right). The field of view is 790 x 540 μm^2. The cross-hair box is about 200 x 200 μm^2. The images are intentionally overexposed, indicating the level of "blooming".

Figure 5: The X-ray penetration into CWO (left), YAG:Ce (center), and Gd_2O_2S:Tb phosphor (right) excited by the 12 keV X-ray minibeam. The view is at 38º with respect to the X-ray beam. Each image is about 340 x 340 μm^2.

Figure 6: On-axis view of the 5 µm x-ray minibeam, using YAG:Ce (left), and CWO (right).The beam intentionally is saturating the camera pixels. Each image is about 340 x 300μm^2.

In Fig. 5, the CWO shows a very small (barely observable) penetration of the X-ray into the crystal. The YAG:Ce (center) image shows a comet-like shape due to significant penetration (~100 µm) of the X-rays into the YAG:Ce scintillator crystal. The phosphor "blooms" and obfuscates the true X-ray beam size or penetration. Fig. 6 shows an on-axis view of the X-ray beam, and is more indicative of the true X-ray beam size, even for the YAG:Ce crystal, even though the pixels were overexposed. In Fig. 7, the pixels are not saturated, and beam profiles were determined in Fig. 8 (and compared to the Au blade scan), and surface plotted in Fig. 9.

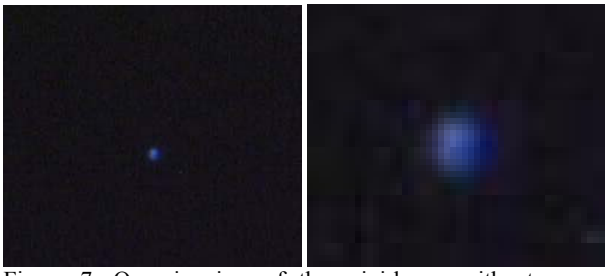

Figure 7: On-axis view of the mini-beam without camera saturation (X-ray intensity adjusted so there are no saturated pixels). The left image covers 340 x 300 μm^2, and the image on the right shows a 66 x 58 μm^2 field of view respectively.

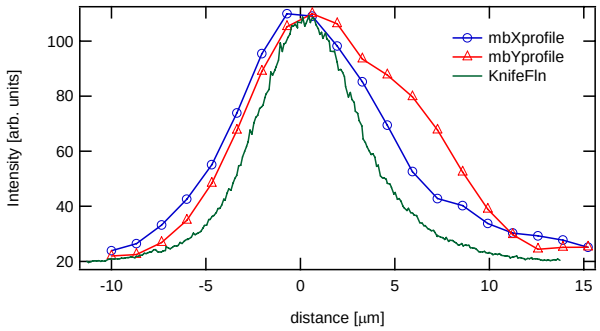

Figure 8: The cross-section of the mini-beam details observed FWHM size of about 8 x 12 μm^2. The fluorescence scan using a 30 nm Au knife edge is shown as solid green line for the horizontal scan direction.

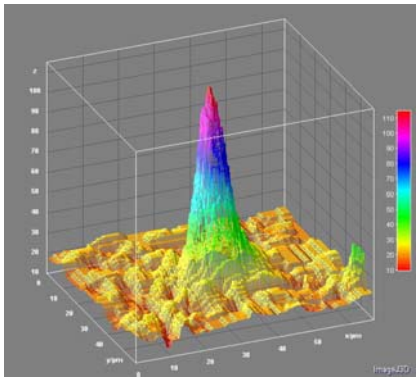

Figure 9: Minibeam surface plot.

We have performed X-ray minibeam visualization at the relatively high photon energy of 12 keV, which is in the vicinity of the Se edge and is the photon energy that is very often used in protein crystallography. Moreover, the X-ray beams at lower energies will be easier to visualize, due to a shorter extinction depth (increased stopping power) of the high-Z $CdWO_4$. This is in agreement with the calculations shown in Fig. 2.

6. X-RAY BEAM: INTENSITY PROFILES

Here we discuss the features of the synchrotron X-ray beam that were observed using a $CdWO_4$ single crystal scintillator, and discuss why they are not observed when Gd_2O_2S:Tb phosphor is used.

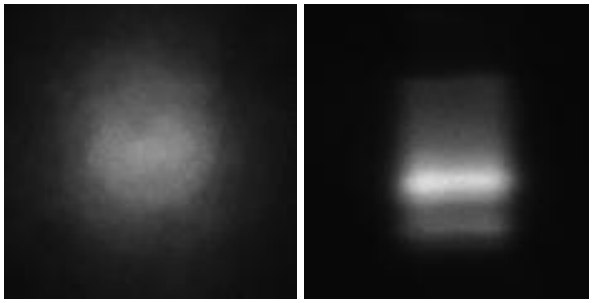

Figure 10: Images of same X-ray beam at the sample location visualized with Gd_2O_2S:Tb phosphor (left), and a single crystal $CdWO_4$ (right) scintillator. Each image is about 150 x 155 μm^2 in size.

The images of the X-ray beam were obtained in on-axis geometry (along the X-ray) direction. The images were collected using a Questar QM-100 microscope, Andor 885 camera (grayscale), and HV-C20 (color images). In order to show the power of the $CdWO_4$ crystal over typical phosphor imaging techniques, we chose to enhance the vertical beam non-uniformity for these measurements. Initially the beam was aligned using only the phosphor as the alignment/diagnostic tool. Afterwards the $CdWO_4$ scintillator was placed at the sample location at 100 K and the measurements repeated. Fig. 10 clearly shows little structure in the beam using the phosphor image. With $CdWO_4$ the resultant image produced both a reliable beam size and an interpretable intensity profile.

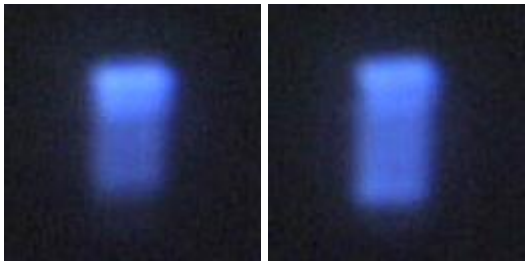

Figure 11: The X-ray beam shape at photon energy 12.7613 keV (left), and 12.6613 keV (right) using a PWO scintillator at 100 K temperature. The field of view is 170 x 170 μm^2.

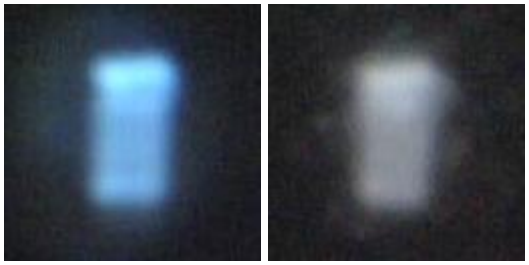

Figure 12: Further comparison of CWO (left) and BGO (right) scintillators at a photon energy of 12.6613 keV and temperature of 100 K. The field of view is 170 x 170 μm^2.

We also undertook studies of the beam shape when photon energy was slightly changed. In Fig. 11 (left) we show that the beam profile can change as energy is changed if the second crystal tune drifts from its optimal setting. This can shift the center of mass of the X-ray beam in such a way that it no longer passes through the center of the omega rotation and the crystal center. The X-ray beam optical center of mass in Fig. 11 shifted vertically by 3 μm, when the photon energy was changed by 100 eV. This indicates a need for optics tuning after changing energy. Such tiny differences are not detected with phosphor, but can be diagnosed with scintillator crystals.

The CWO and BGO scintillators (Fig. 12) have compatible light output but are brighter than PWO by an order of magnitude at temperatures near 100 K; however, since we are interested in visualization of the primary X-ray beam, PWO scintillation is intense enough to be useful, yet PWO has the highest x-ray absorption and best imaging resolution. The resolution of the beam edges with the PWO scintillator is limited by our camera capabilities and is better than 2 μm. The attenuator settings for PWO were set at 2.89, while for CWO and BGO it was set to 23 for the images collected above. It is worth noting that the surface quality of a CWO crystal is generally not as good as PWO due to the [010] cleavage plane in CWO. The PWO emission is dark blue, while CWO has a light blue emission and BGO has a white emission color.

7. RESULTS AND DISCUSSION

A high-Z scintillator such as CWO has a short absorption depth and little "blooming," which allows detailed imaging of the X-ray synchrotron beam even at high photon energies. The ideal imaging of the X-ray beam is on-axis (along the X-ray beam), due to the 3D nature of the excited fluorescence source. Despite the fact that we used a photon energy just above L3 and L2 (below L1) edges of W, we observed an insignificant amount of "blooming" from CWO and PWO crystal scintillators.

8. SOFTWARE: X-RAY BEAM CENTERING

Using the CWO scintillator crystal, we have developed software that characterizes synchrotron X-ray beam properties. Of particular interest is the location of the center of the X-ray beam, beam size, and beam center of gravity.

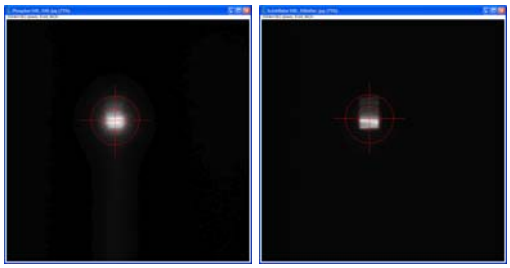

Figure 13: Software determines the position of the center of mass of the X-ray beam for phosphor (left), and the single crystal CWO scintillator (right). The center of mass was used in drawing the cross-hair.

	Area	XM	YM	Width	Height
1	5261	448.348	409.901	79	88
2	2868	450.377	409.391	53	66

Table 4: Software determines the X-ray beam parameters for phosphor (1=left image), and the CWO single crystal scintillator (2=right image). These values are determined in pixels.

9. CONCLUSIONS

We demonstrated that a single CWO crystal scintillator can be used to effectively image beam size, intensity profile and the fine structure of micrometer size X-ray beams at synchrotron beamlines. This is a significant improvement for X-ray synchrotron beam diagnostics and imaging over the currently used phosphors, especially when using on-axis viewing. Our approach determines not only X-ray beam shape, but also intensity distribution and fine beam structure. The practical scintillator crystal tool opens a simple way to characterize synchrotron beam properties at the sample position quickly. The single crystal scintillator imager has also an application in the alignment of mini and micro beam collimators.

The CWO-based X-ray beam imager is a non-hygroscopic single crystal scintillator with a high effective Z, a large X-ray absorption cross section in the photon energy, negligible radiation damage and a very high index of refraction. Two other scintillator crystals also can be used for these purposes (PWO and BGO). These X-ray, optical, and mechanical characteristics allow efficient conversion of X-ray into visible light within a short scintillator thickness and imaging the visible light with conventional visible light optics and cameras. We find that at a temperature of 100 K, PWO shows the best X-ray beam image quality despite reduced scintillator efficiency, followed by CWO and BGO.

10. ACKNOWLEDGEMENTS

The authors are indebted to Andor Technology Inc. for the camera loan. We would also like to thank Norma Duke for beamline setup, Randy Alkire for the Au blade scan of the minibeam and many helpful discussions regarding beamline optics, Mike Molitsky for making high precision pins, and Michelle Radford, Lindsey Butler and Frank Rotella for reviewing the manuscript.

This work was supported by the U. S. Department of Energy, Office of Biological and Environmental Research and Office of Basic Energy Sciences, under Contract DE-AC02-06CH11357.

11. REFERENCES

[1] X. Vernede, B. Lavault, J. Ohana, D. Nurizzo, J. Joly, L. Jacquamet, F. Felisaz, F. Cipriani, D. Bourgeois. "UV laser-excited fluorescence as a tool for the visualization of protein crystals mounted in loops." *Acta Cryst*. (2006). **D62**, 253–261.

[2] R. Sanishvili, V. Nagarajan, D. Yoder, M. Becker, S. Xu, S. Corcoran, D. L. Akey, J. L. Smith, and R. F. Fischetti. "A 7 μm mini-beam improves diffraction data from small or imperfect crystals of macromolecules" *Acta Cryst*. (2008). **D64**, 425–435.

[3] G. Rosenbaum, R. W. Alkire, G. Evans, F. J. Rotella, K. Lazarski, R.-G. Zhang, S. L. Ginell, N. Duke, I. Naday, J. Lazarz, M. J. Molitsky, L. Keefe, J. Gonczy, L. Rock, R. Sanishvili, M. A. Walsh, E. Westbrook and A. Joachimiak, "The Structural Biology Center 19ID undulator beamline: facility specifications and protein crystallographic results" *J. Synchrotron Rad.* (2006). **13**, 30–45.

[4] A. Perrakis, F. Cipriani, J. Castagna, L. Claustre, M. Burghammer, C. Riekel, and S. Cusack, "Protein microcrystals and the design of a micro-diffractometer: current experience and plans at EMBL and ESRF/ID13." *Acta Cryst*. (1999). **D55**, 1765–1770. We believe that authors used $Bi_4Ge_3O_{12}$ and not $B_{14}Ge_3O_{12}$ that is discussed in their publication.

[5] E. Girard, P. Legrand, O. Roudenko, L. Roussier, P. Gourhant, J. Gibelin, D. Dalle, M. Ounsy, A. W. Thompson, O. Svensson, M-O Cordier, S. Robin, R. Quiniou, and J-P. Steyer "Instrumentation for synchrotron-radiation macromolecular crystallography", *Acta Cryst*. (2006). **D62**, 12–18.

[6] K. J. Gofron et al., "On-Axis optics for sample visualization - biological crystals and synchrotron beams imaging". In preparation.

[7] List of scintillators and published references are at http://scintillator.lbl.gov/ .

[8] O. Paris, C. Li, S. Siegel, G. Weseloh, F. Emmerling, H. Riesemeier, A. Erko and P. Fratzl, "A new experimental station for simultaneous X-ray microbeam scanning for small- and wide-angle scattering and fluorescence at BESSY II." *J. Appl. Cryst*. (2007). **40**, s466–s470.

[9] J. M. Yi, Y. S. Chu, T. S. Argunova, and J. H. Je, "Analytic determination of the three-dimensional distribution of dislocations using synchrotron X-ray topography." *J. Appl. Cryst*. (2006). **39**, 106–108.

[10] J. M. Yi, Y. S. Chu, Y. Zhong, J. H. Je, Y. Hwu and G. Margaritondo, "X-ray bright-field imaging analyzes crystalline quality and defects of SiC wafers." *J. Appl. Cryst*. (2007). **40**, 376–378.

[11] V. V. Laguta, M. Nikl, and S. Zazubovich, "Physics of Lead Tungstate Scintillators" *IEEE Trans. Nucl. Sci.*, (2008), **55**(3-2), 1275–1282.

[12] A.A. Annenkov, M.V. Korzhik, P. Lecoq, ”Lead tungstate scintillation material.” *Nucl. Instrum. Methods,* (2002), A490(1-2), 30–50.
[13] R.W. Novotny, S. F. Burachas, W. M. Döring, V. Dormenev, Y. M. Goncharenko, M. S. Ippolitov, A. Hofstaetter, M. Korzhik, V. Manko, Y. M. Melnik, O. Missevitch, V. V. Mochalov, A. V. Ryazantsev, P. A. Semenov, G. Tamulaitis, A. V. Uzunian, A. A. Vasiliev, and A. N. Vasiliev, ”Radiation Hardness and Recovery Processes of PWO Crystals at -25ºC” *IEEE Trans. Nucl. Sci*. (2008), 55(3-2), 1283–1288.
[14] B.C. Grabmaier, “Crystal Scintillators” *IEEE Trans. Nucl. Sci.,* (1984), **NS-31**(1), 372–376.
[15] XOP http://www.esrf.eu/UsersAndScience/Experiments/TBS/SciSoft/xop2.3 .
[16] IIT http://www.csrri.iit.edu/mucal.html
[17] Saint-Gobain http://www.detectors.saint-gobain.com/$CdWO_4$.aspx.